

Observational Constraints on Oscillating Dark-Energy Parametrizations

Supriya Pan^a Emmanuel N. Saridakis^{b,c,d} Weiqiang Yang^e

^a*Department of Mathematics, Raiganj Surendranath Mahavidyalaya, Sudarshanpur, Raiganj, Uttar Dinajpur, West Bengla 733134, India*

^b*Chongqing University of Posts & Telecommunications, Chongqing, 400065, China*

^c*Physics Division, National Technical University of Athens, 15780 Zografou Campus, Athens, Greece*

^d*CASPER, Physics Department, Baylor University, Waco, TX 76798-7310, USA*

^e*Department of Physics, Liaoning Normal University, Dalian, 116029, P. R. China*

E-mail: span@research.jdvu.ac.in, Emmanuel_Saridakis@baylor.edu, d11102004@163.com

ABSTRACT: We perform a detailed confrontation of various oscillating dark-energy parametrizations with the latest sets of observational data. In particular, we use data from Joint Light Curve analysis (JLA) sample from Supernovae Type Ia, Baryon Acoustic Oscillations (BAO) distance measurements, Cosmic Microwave Background (CMB) observations, redshift space distortion, weak gravitational lensing, Hubble parameter measurements from cosmic chronometers, and the local Hubble constant value, and we impose constraints on four oscillating models. We find that all models are bent towards the phantom region, nevertheless in the three of them the quintessential regime is also allowed within 1σ confidence-level. Furthermore, the deviations from Λ CDM cosmology are small, however for two of the models they could be visible at large scales, through the impact on the temperature anisotropy of the CMB spectra and on the matter power spectra.

KEYWORDS: Dark Energy, Observational Constraints, Oscillating Parametrizations

Contents

1	Introduction	1
2	Cosmological equations: Background and perturbations	2
3	Oscillating Dark-Energy models	4
4	Observational Data	5
5	Observational constraints	6
5.1	Model I	7
5.2	Model II	9
5.3	Model III	10
5.4	Model IV	12
6	Model comparison	14
7	Conclusions	15

1 Introduction

The universe acceleration at late times is one of the most interesting findings of modern cosmology, and thus there are two main directions that one could follow to explain it. The first way is to keep general relativity as the gravitational theory and introduce new components, that go beyond the Standard Model of Particle Physics, collectively known as the dark energy sector [1, 2]. The second way is to construct a modified gravitational theory, whose additional degrees of freedom can drive the universe acceleration [3–5].

At the phenomenological level both the above approaches lead to a specific universe accelerated expansion, that can be quantified by the evolution of the (effective in the case of modified gravity) dark energy equation-of-state parameter. Hence, parametrizations of the dark energy fluid can lead to reconstructions of the universe late-time expansion. The basic idea relies on the fact that the dark energy equation-of-state parameter $w_x = p_x/\rho_x$, with ρ_x and p_x the dark energy energy density and pressure respectively, can be parametrized using different functional forms in terms of the cosmological redshift.

In principle, there is not a theoretical guiding rule to select the best $w_x(z)$, however using observational data it is possible to find viable parametrizations. In the literature one can find many parametric dark energy models, that have been introduced and fitted with observational data: (i) one-parameter family of dark energy models [6] (ii) two-parameters family of dark energy parametrizations, namely, Chevallier-Polarski-Linder parametrization [7, 8], Linear parametrization [9–11], Logarithmic parametrization

[12], Jassal-Bagla-Padmanabhan parametrization [13], Barboza-Alcaniz parametrization [14], etc (see [15–19]), (iii) three-parameters family of dark energy parametrizations [20], and (iv) four-parameters family of dark energy parametrizations [20–22].

One of the interesting parametrizations is the class of models in which $w_x(z)$ exhibits oscillating behaviour [19, 23–28]. The oscillating dark energy models are appealing and prove to lead to desirable cosmological behavior. In particular, they can alleviate the coincidence problem, since they may lead to both accelerating and decelerating phases in a periodic manner [24], and thus to dark matter and dark energy density parameters of the same order. Furthermore, one can construct oscillating dark energy models that can unify the current acceleration with the early-time inflationary phase [25].

The main question that arises naturally is whether oscillating dark-energy models are in agreement with the latest observational data. Although an early, basic fitting was performed in [29], such an investigation has not been fulfilled in detail. In the present work we are interested in performing a complete observational confrontation, in order to examine whether oscillating dark energy models are in agreement with the latest data, namely: Joint Light Curve analysis sample from Supernovae Type Ia, Baryon Acoustic Oscillations (BAO) distance measurements, Cosmic Microwave Background (CMB) observations, redshift space distortion, weak gravitational lensing, Hubble parameter measurements from cosmic chronometers, and finally the local Hubble constant value.

The manuscript is organized in the following way. In Section 2 we present the cosmological equations for a dark energy model, both at background and perturbative levels. In Section 3 we introduce the oscillating dark energy models, through suitable parametrizations of the dark-energy equation-of-state parameter. In Section 4 we present the various observational data sets that we will use in our analysis, and in Section 5 we perform a detailed observational confrontation for various oscillating models. In Section 6 we compare the results for all models, both amongst each other as well as relating to w CDM and Λ CDM cosmology. Finally, Section 7 is devoted to the Conclusions.

2 Cosmological equations: Background and perturbations

In this section we provide the basic equations, both at the background and at the perturbation level, of a general cosmological scenario. Throughout the work we consider the homogeneous and isotropic Friedmann-Lemaître-Robertson-Walker (FLRW) metric of the form

$$ds^2 = -dt^2 + a^2(t) \left[\frac{dr^2}{1 - kr^2} + r^2 (d\theta^2 + \sin^2 \theta d\phi^2) \right], \quad (2.1)$$

where $a(t)$ is the scale factor and $k = -1, +1, 0$ corresponds respectively to open, closed and flat geometry. For simplicity, in the following we focus on the flat geometry, as it is favored by observations, although the analysis can be straightforwardly extended to the non-flat case too. The Friedmann equations are extracted as

$$H^2 + \frac{k}{a^2} = \frac{8\pi G}{3} \rho_{tot}, \quad (2.2)$$

$$2\dot{H} + 3H^2 + \frac{k}{a^2} = -8\pi G p_{tot}, \quad (2.3)$$

where $H = \dot{a}/a$ is the Hubble function and dots denote derivatives with respect to the cosmic time, t . In the above equations ρ_{tot} and p_{tot} are respectively the total energy density and pressure of the universe content, considered to be effectively described by perfect fluids. In particular, we consider that the universe consists of radiation, baryonic matter, dark matter and (effective) dark energy, and therefore the total energy density and the total pressure of the universe read as $\rho_{tot} = \rho_r + \rho_b + \rho_c + \rho_x$ and $p_{tot} = p_r + p_b + p_c + p_x$, where ρ_r, p_r correspond to radiation, ρ_b, p_b to baryonic sector, ρ_c, p_c to dark matter, and ρ_x, p_x to the dark energy sector. If we additionally assume that these sectors do not mutually interact, then each one is separately conserved, namely it satisfies

$$\dot{\rho}_i + 3H(1 + w_i)\rho_i = 0, \quad (2.4)$$

where $w_i \equiv p_i/\rho_i$ is the i -th component's equation-of-state parameter. Since radiation has $w_r = 1/3$, we obtain $\rho_r \propto (a/a_0)^{-4}$. Similarly, since as usual the baryonic and dark matter sectors are considered to be pressureless, we obtain $\rho_b \propto (a/a_0)^{-3}$ and $\rho_c \propto (a/a_0)^{-3}$, with a_0 the current value of the scale factor. Finally, since the dark energy fluid has a general equation-of-state parameter $w_x \equiv p_x/\rho_x$, its evolution equation leads to

$$\rho_x = \rho_{x,0} \left(\frac{a}{a_0}\right)^{-3} \exp\left(-3 \int_{a_0}^a \frac{w_x(a')}{a'} da'\right). \quad (2.5)$$

Hence, we can see that the evolution of the dark energy fluid is obviously highly dependent on the form of $w_x(a)$.

Let us now investigate the perturbations of the above general cosmological scenario. The perturbation equations of a general dark energy scenario have been explored in detail in the literature [1]. We choose the synchronous gauge, and thus the perturbed FLRW metric takes the form

$$ds^2 = a^2(\tau) [-d\tau^2 + (\delta_{ij} + h_{ij})dx^i dx^j], \quad (2.6)$$

where τ is the conformal time, and where δ_{ij}, h_{ij} are respectively the unperturbed and the perturbed metric tensors. Now, for the perturbed FLRW metric (2.6), using the conservation equation for the energy-momentum tensor of the i -th fluid, namely $T_{;\nu}^{\mu\nu} = 0$, one can obtain the continuity and the Euler equations for a mode with wavenumber κ , in the synchronous gauge, as [30–32]:

$$\delta'_i = -(1 + w_i) \left(\theta_i + \frac{h'}{2}\right) - 3\mathcal{H} \left(\frac{\delta p_i}{\delta \rho_i} - w_i\right) \delta_i - 9\mathcal{H}^2 \left(\frac{\delta p_i}{\delta \rho_i} - c_{a,i}^2\right) (1 + w_i) \frac{\theta_i}{\kappa^2}, \quad (2.7)$$

$$\theta'_i = -\mathcal{H} \left(1 - 3 \frac{\delta p_i}{\delta \rho_i}\right) \theta_i + \frac{\delta p_i / \delta \rho_i}{1 + w_i} \kappa^2 \delta_i - \kappa^2 \sigma_i, \quad (2.8)$$

where the prime denotes differentiation with respect to the conformal time τ . In these equations $\delta_i = \delta\rho_i/\rho_i$ is the density perturbation, $\mathcal{H} = a'/a$, is the conformal Hubble factor, $h = h_j^j$ is the trace of the metric perturbations h_{ij} , and $\theta_i \equiv i\tilde{\kappa}^j v_j$ is the divergence

of the i -th fluid velocity. Additionally, σ_i is the anisotropic stress of the i -th fluid, which will be neglected in our analysis. Finally, $c_{a,i}^2 = \dot{p}_i/\dot{\rho}_i$ is the adiabatic speed of sound of the i -th fluid. As it is known, for an imperfect fluid the quantity $c_s^2 = \delta p_i/\delta \rho_i$ is the sound speed for the i -th fluid. Thus, the adiabatic sound speed is related to the sound speed through

$$c_{a,i}^2 = w_i - \frac{w_i'}{3\mathcal{H}(1+w_i)}. \quad (2.9)$$

We mention here that many dark energy models can be described through imperfect fluids, which have $c_s^2 = 1$ while c_a could be different [33–35]. Hence, although there exist models with $c_s^2 > 1$ (e.g in k -essence models), in our analysis we fix this quantity to be unity.

3 Oscillating Dark-Energy models

In this section we consider dark energy parametrizations that exhibit oscillating behaviour with the evolution of the universe. Our primary intention is to investigate these models with current cosmological data. Two models that present oscillatory behavior are [27]

$$w_x(a) = -\cos \left[b \ln \left(\frac{a}{a_0} \right) \right], \quad (3.1)$$

$$w_x(a) = w_0 - A \sin \left[B \ln \left(\frac{a}{a_0} \right) \right], \quad (3.2)$$

where b , w_0 , A , B are the involved free parameters. One can easily see that the current value of the dark-energy equation of state, namely at $a = a_0$, in model (3.1) is $w_x(a_0) = -1$, while in model (3.2) is w_0 .

In the present work we proceed to generalizations of the above models. For convenience we will use as independent variable the redshift, defined as $z = \frac{a_0}{a} - 1$, with the current scale factor set to 1 for simplicity. We will study the following four models:

- Model I

A first generalization of (3.1) is to consider

$$w_x(z) = w_0 + b \{1 - \cos [\ln(1+z)]\}, \quad (3.3)$$

where w_0 is the current value of $w_x(z)$ and b is the model parameter. The free parameter b quantifies the dynamical character of the model. For $b = 0$ we acquire $w_x(z) = w_0$, while any nonzero value of b corresponds to a deviation of the model from the constant dark-energy equation-of-state parameter. One important advantage of this model is that the current value of the dark-energy equation-of-state parameter can be free.

- Model II

In similar lines we can slightly extend model (3.2) as

$$w_x(z) = w_0 + b \sin [\ln(1+z)], \quad (3.4)$$

with w_0 and b the model parameters.

- Model III

Another oscillatory dark energy parametrization is [19]

$$w_x(z) = w_0 + b \left[\frac{\sin(1+z)}{1+z} - \sin 1 \right], \quad (3.5)$$

with w_0 and b the model parameters.

- Model IV

Finally, we consider the model

$$w_x(z) = w_0 + b \left[\frac{z}{1+z} \right] \cos(1+z). \quad (3.6)$$

4 Observational Data

In this section we provide the various data sets that we will incorporate in the observational fittings. We will use data from the following probes:

1. *Supernovae Type Ia*: We include the latest Joint Light Curve analysis sample [36] from Supernovae Type Ia, one of the cosmological data sets to probe the nature of dark energy. The sample contains 740 number of Supernovae Type Ia data, distributed in the redshift interval $z \in [0.01, 1.30]$.
2. *Baryon Acoustic Oscillations (BAO) distance measurements*: We include four BAO sets, namely the 6dF Galaxy Survey (6dFGS) measurement at $z_{\text{eff}} = 0.106$ [37], the Main Galaxy Sample of Data Release 7 of Sloan Digital Sky Survey (SDSS-MGS) at $z_{\text{eff}} = 0.15$ [38], and the CMASS and LOWZ samples from the latest Data Release 12 (DR12) of the Baryon Oscillation Spectroscopic Survey (BOSS) at $z_{\text{eff}} = 0.57$ and at $z_{\text{eff}} = 0.32$ [39].
3. *Cosmic Microwave Background (CMB) data*: We incorporate the cosmic microwave background data from [40, 41] which combine the likelihoods C_l^{TT} , C_l^{EE} , C_l^{TE} in addition to the low- l polarization. Notationally, this data is recognized by Planck TT, TE, EE + lowTEB.
4. *Redshift space distortion*: We include two redshift space distortion (RSD) data from CMASS and LowZ galaxy samples. The CMASS sample consists of 777202 galaxies with an effective redshift of $z_{\text{eff}} = 0.57$ [39], while the LOWZ sample contains 361762 galaxies with an effective redshift of $z_{\text{eff}} = 0.32$ [39].
5. *Weak lensing data*: We consider the weak gravitational lensing (using the blue galaxy sample) from the Canada–France–Hawaii Telescope Lensing Survey (CFHTLenS) [42, 43].

6. *Cosmic Chronometers (CC) data:* In our analysis we consider the Hubble parameter values at different redshifts using the massive and passively evolving galaxies in our universe. These galaxies are known as cosmic chronometers, the measurements of the Hubble parameter values follow the spectroscopic method with high accuracy, and moreover the technique of measurements is model independent [44, 45]. The CC (or $H(z)$) data are compiled in [46] and are distributed in the interval $0 < z < 2$ and contains 30 measurements.
7. *Local Hubble constant:* The latest and improved value of the local Hubble constant yielding $H_0 = 73.24 \pm 1.74 \text{ km s}^{-1} \text{ Mpc}^{-1}$ at 2.4% precision has been reported by Riess et al. [47] (we call this data as R16). The reduction of the uncertainty (from 3.3% to 2.4%) in the measurement of H_0 appears using the Wide Field Camera 3 (WFC3) on the Hubble Space Telescope (HST).

5 Observational constraints

In this section we proceed to the detailed confrontation of the above oscillating dark energy models with observational data. We perform a combined analysis JLA + BAO + Planck TT, TE, EE + LowTEB (CMB) + RSD + WL+ CC + R16 to constrain the proposed oscillating dark energy models (3.3), (3.4), (3.5) and (3.6). Our analysis follows the likelihood $\mathcal{L} \propto \exp(-\chi^2/2)$, where

$$\chi^2 = \chi_{JLA}^2 + \chi_{BAO}^2 + \chi_{CMB}^2 + \chi_{RSD}^2 + \chi_{WL}^2 + \chi_{CC}^2 + \chi_{R16}^2. \quad (5.1)$$

The main statistical analysis is based on the ‘‘Code for Anisotropies in the Microwave Background’’ (CAMB) [48], a publicly available code. For each of the studied models we modify the code accordingly, and then we additionally use CosmoMC, a Markov Chain Monte Carlo (MCMC) simulation, in order to extract the cosmological constraints for the oscillating dark energy models. In summary, we analyze the following eight-dimensional parameters space:

$$\mathcal{P}_1 \equiv \left\{ \Omega_b h^2, \Omega_c h^2, 100\theta_{MC}, \tau, w_0, b, n_s, \log[10^{10} A_s] \right\}, \quad (5.2)$$

where $\Omega_b h^2$, $\Omega_c h^2$ are respectively the baryon and the cold dark matter density parameter, $100\theta_{MC}$ and τ refer respectively to the ratio of the sound horizon to the angular diameter distance and to the optical depth, n_s and A_s are respectively the scalar spectral index and the amplitude of the initial power spectrum [40], and w_0 and b are the free parameters of the oscillating dark energy models. Additionally, the priors on the cosmological parameters used in the analysis are displayed in Table 1. Lastly, in the following the subscript ‘‘0’’ denotes the value of a quantity at present.

In the next subsections we describe the obtained results on each model from this combined analysis.

Parameter	Prior
$\Omega_c h^2$	[0.01, 0.99]
$\Omega_b h^2$	[0.005, 0.1]
$100\theta_{MC}$	[0.5, 10]
τ	[0.01, 0.8]
n_s	[0.5, 1.5]
$\log[10^{10} A_s]$	[2.4, 4]
w_0	[-2, 0]
b	[-3, 3]

Table 1. The flat priors on the cosmological parameters for the CosmoMC analysis.

5.1 Model I

We perform the above combined analysis for the Model I of (3.3), and in Table 2 we summarize the main observational constraints. Furthermore, in Fig. 1 we present the 1σ and 2σ confidence-level contour plots for several combinations of the model parameters and of the derived parameters. Similarly, in Fig. 2 we display the marginalized one-dimensional posterior distributions for the involved quantities.

Parameters	Mean $\pm 1\sigma \pm 2\sigma \pm 3\sigma$	Best fit
$\Omega_c h^2$	0.1188 ^{+0.0013+0.0024+0.0031} _{-0.0013-0.0024-0.0031}	0.1190
$\Omega_b h^2$	0.02227 ^{+0.00015+0.00030+0.00038} _{-0.00015-0.00029-0.00038}	0.02227
$100\theta_{MC}$	1.04056 ^{+0.00033+0.00058+0.00075} _{-0.00030-0.00060-0.00075}	1.04042
τ	0.061 ^{+0.017+0.035+0.042} _{-0.018-0.033-0.051}	0.074
n_s	0.9745 ^{+0.0041+0.0081+0.0107} _{-0.0041-0.0079-0.0100}	0.9792
$\ln(10^{10} A_s)$	3.062 ^{+0.033+0.067+0.090} _{-0.033-0.067-0.086}	3.087
w_0	-1.0267 ^{+0.0296+0.0488+0.0761} _{-0.0204-0.0643-0.0769}	-1.0141
b	-0.2601 ^{+0.3235+0.4567+0.5132} _{-0.1513-0.6028-0.9237}	-0.4234
Ω_{m0}	0.298 ^{+0.007+0.016+0.021} _{-0.008-0.015-0.018}	0.299
σ_8	0.824 ^{+0.014+0.028+0.036} _{-0.014-0.030-0.037}	0.838
H_0	68.95 ^{+0.93+1.68+1.96} _{-0.70-1.84-2.47}	68.93

Table 2. Summary of the observational constraints on Model I of (3.3), using the observational data JLA + BAO + Planck TT, TE, EE + LowTEB + RSD + WL+ CC + R16. We define $\Omega_{m0} = \Omega_{c0} + \Omega_{b0}$ and we use H_0 to denote the current value of the Hubble function.

Our analysis reveals that both the best-fit and the mean values of the dark energy equation-of-state parameter at present (w_0) exhibit phantom behaviour although very close to the cosmological constant boundary, however, as one can see from Table 2, within 1σ confidence-region the quintessential character of w_0 is not excluded.

Additionally, we analyze the behaviour of Model I at large scales through its impact on the temperature anisotropy of the CMB spectra and on the matter power spectra, shown respectively in the upper and lower panel of the Fig. 3, and moreover we compare the

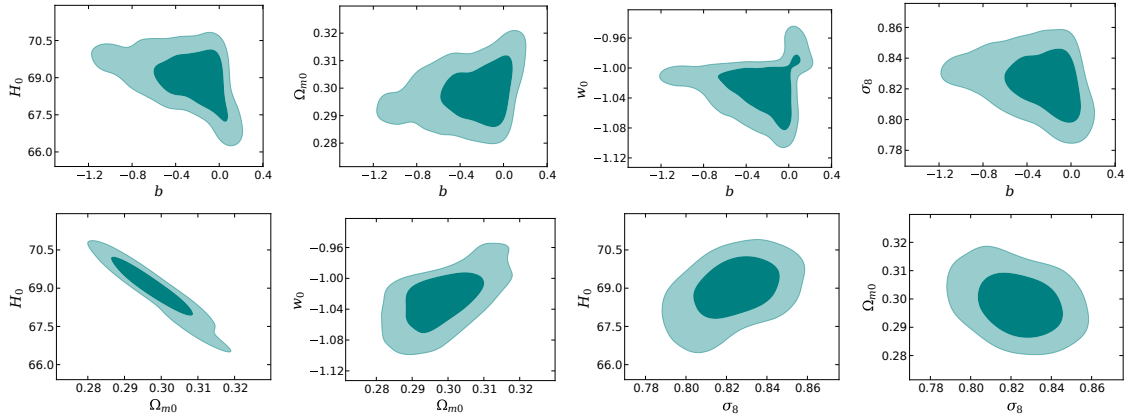


Figure 1. 1σ (68.3%) and 2σ (95.4%) confidence level contour plots for different combinations of the model parameters of Model I (3.3), for the combined observational data JLA + BAO + Planck TT, TE, EE + LowTEB + RSD + WL+ CC + R16. We have defined, $\Omega_{m0} = \Omega_{c0} + \Omega_{b0}$.

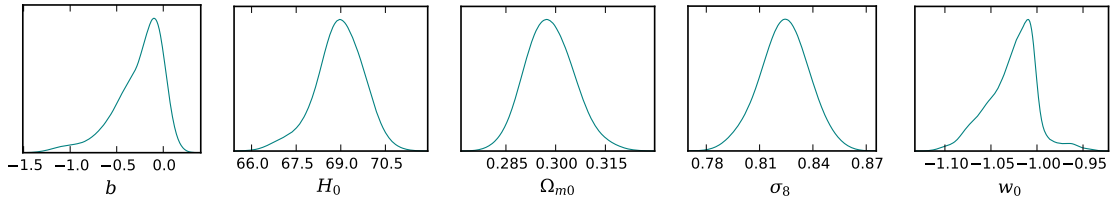


Figure 2. The marginalized 1-dimensional posterior distributions for the model parameters of Model I of (3.3), for the combined observational data JLA + BAO + Planck TT, TE, EE + LowTEB + RSD + WL+ CC + R16.

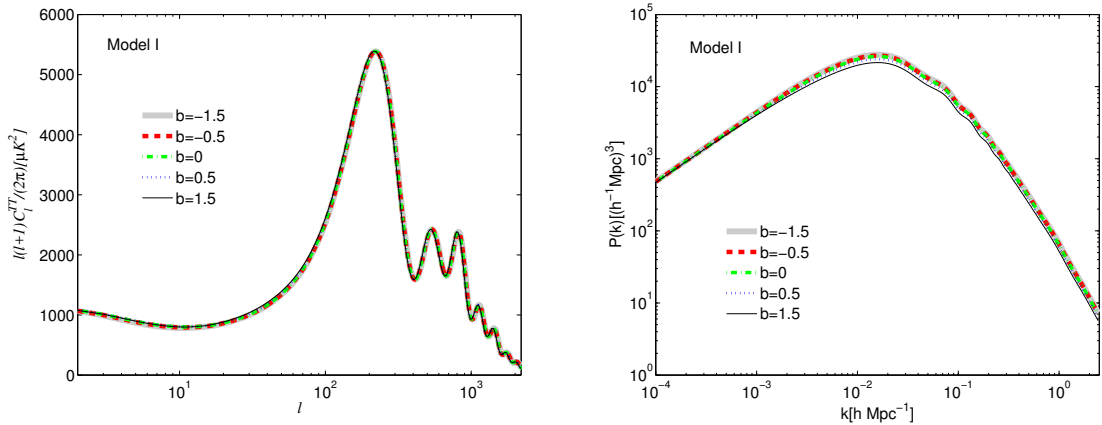


Figure 3. The temperature anisotropy in the CMB spectra (left panel) and the matter power spectra (right panel), for Model I of (3.3), for different values of the parameter b .

results with w CDM cosmology (obtained for $b = 0$). We find that for several values of b we do not find a remarkable behaviour in the CMB spectra. On the other hand, from the matter power spectra we can see that for large positive b values the model has a deviating

nature from w CDM cosmology.

In summary, from the observational constraints we deduce that the model is close to w CDM cosmology, and hence to the Λ CDM paradigm too.

5.2 Model II

We perform the combined analysis for the Model II of (3.4), and in Table 3 we summarize the main observational constraints. Additionally, in Fig. 4 we depict the 1σ and 2σ confidence-level contour plots for several combinations of the model parameters and the derived parameters, while in Fig. 5 we display the corresponding marginalized one-dimensional posterior distributions for the involved quantities.

Parameters	Mean $\pm 1\sigma \pm 2\sigma \pm 3\sigma$	Best fit
$\Omega_c h^2$	$0.1185^{+0.0012+0.0022+0.0029}_{-0.0012-0.0023-0.0032}$	0.1173
$\Omega_b h^2$	$0.02227^{+0.00015+0.00029+0.00039}_{-0.00015-0.00028-0.00038}$	0.02244
$100\theta_{MC}$	$1.04058^{+0.00031+0.00060+0.00077}_{-0.00031-0.00063-0.00084}$	1.04068
τ	$0.063^{+0.017+0.034+0.048}_{-0.017-0.032-0.046}$	0.067
n_s	$0.9752^{+0.0040+0.0084+0.0109}_{-0.0044-0.0078-0.0098}$	0.9793
$\ln(10^{10} A_s)$	$3.065^{+0.033+0.064+0.090}_{-0.033-0.064-0.091}$	3.074
w_0	$-1.0517^{+0.0301+0.0979+0.1285}_{-0.0362-0.0744-0.1049}$	-1.0645
b	$0.0113^{+0.0299+0.0837+0.1333}_{-0.0457-0.0738-0.0834}$	0.0422
Ω_{m0}	$0.297^{+0.007+0.016+0.022}_{-0.009-0.016-0.018}$	0.288
σ_8	$0.823^{+0.015+0.028+0.035}_{-0.015-0.028-0.036}$	0.824
H_0	$69.02^{+0.95+1.73+2.08}_{-0.73-1.98-2.62}$	69.77

Table 3. Summary of the observational constraints on Model II of (3.4) using the observational data JLA + BAO + Planck TT, TE, EE + LowTEB + RSD + WL+ CC + R16.

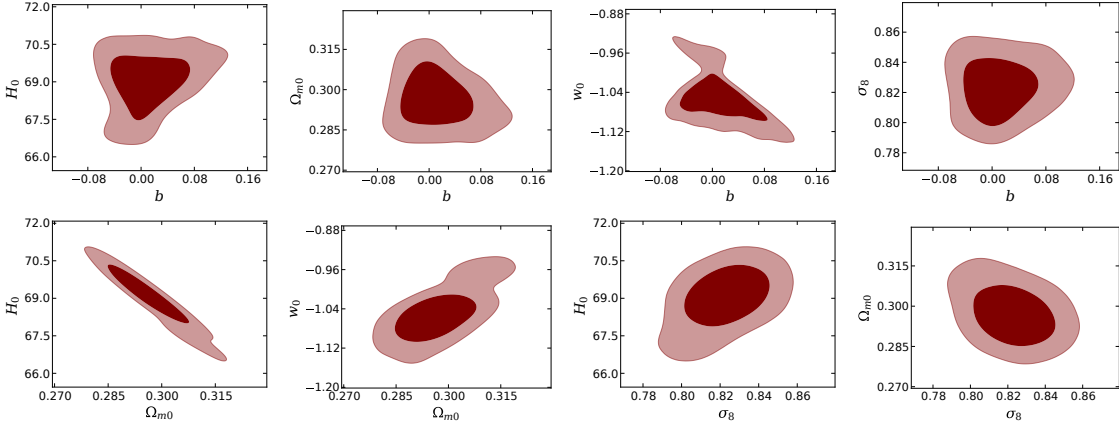


Figure 4. 1σ (68.3%) and 2σ (95.4%) confidence level contour plots for different combinations of the model parameters of Model II of (3.4), for the combined observational data JLA + BAO + Planck TT, TE, EE + LowTEB + RSD + WL+ CC + R16.

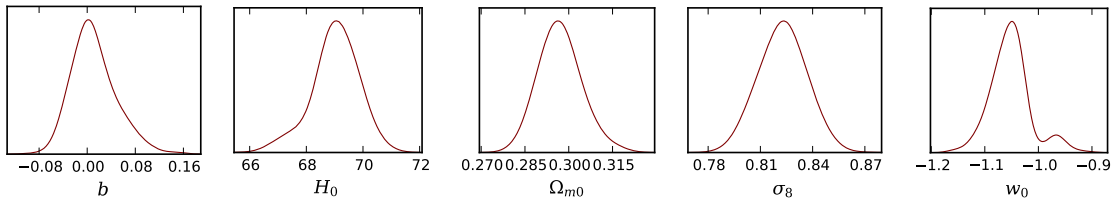


Figure 5. The marginalized 1-dimensional posterior distributions for the model parameters of Model II of (3.4), for the combined observational data JLA + BAO + Planck TT, TE, EE + LowTEB + RSD + WL+ CC + R16.

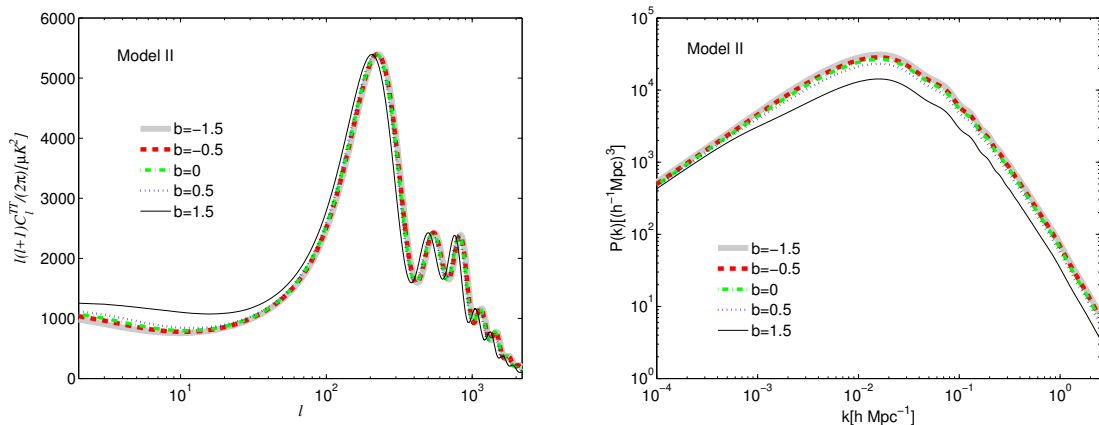


Figure 6. The temperature anisotropy in the CMB spectra (left panel) and the matter power spectra (right panel), for Model II of (3.4), for different values of the parameter b .

The joint analysis on Model II shows that the best-fit and the mean values of the current value of the dark energy equation-of-state parameter w_0 lie strongly in the phantom regime (at 1σ confidence-level w_0 is strictly less than -1). However, as we can see from Table 3, w_0 is close to the cosmological constant boundary. Additionally, from the temperature anisotropy in the CMB spectra and the matter power spectra depicted in Fig. 6, we can observe that at large scales this model exhibits a clear deviation from w CDM cosmology (and thus Λ CDM cosmology too) for large positive values of the parameter b .

5.3 Model III

We perform the combined analysis described above, for the Model III of (3.5), and in Table 4 we give the summary of the main observational constraints. Furthermore, in Fig. 7 we present the 1σ and 2σ confidence-level contour plots for several combinations of the model parameters and of the derived parameters. Additionally, in Fig. 8 we display the corresponding marginalized one-dimensional posterior distributions for the involved quantities.

According to the joint analysis we find that for Model III, both the best fit and the mean values of the dark-energy equation-of-state parameter at present exhibit phantom behaviour, although very close to the cosmological constant boundary, nevertheless, as

Parameters	Mean $\pm 1\sigma \pm 2\sigma \pm 3\sigma$	Best fit
$\Omega_c h^2$	$0.1184^{+0.0014+0.0025+0.0029}_{-0.0012-0.0026-0.0032}$	0.1178
$\Omega_b h^2$	$0.02228^{+0.00014+0.00030+0.00039}_{-0.00014-0.00028-0.00039}$	0.02234
$100\theta_{MC}$	$1.04062^{+0.00033+0.00064+0.00081}_{-0.00034-0.00061-0.00083}$	1.04074
τ	$0.065^{+0.018+0.037+0.047}_{-0.018-0.038-0.050}$	0.057
n_s	$0.9756^{+0.0043+0.0087+0.0119}_{-0.0045-0.0082-0.0105}$	0.9764
$\ln(10^{10} A_s)$	$3.070^{+0.034+0.070+0.091}_{-0.034-0.074-0.095}$	3.052
w_0	$-1.0079^{+0.0554+0.1367+0.1866}_{-0.0731-0.1172-0.1531}$	-1.0411
b	$0.1542^{+0.2478+0.7666+1.0573}_{-0.3864-0.6304-0.7418}$	-0.0914
Ω_{m0}	$0.301^{+0.008+0.016+0.021}_{-0.008-0.016-0.022}$	0.299
σ_8	$0.821^{+0.013+0.025+0.033}_{-0.013-0.026-0.034}$	0.808
H_0	$68.59^{+0.84+1.68+2.32}_{-0.83-1.58-2.13}$	68.66

Table 4. Summary of the observational constraints on Model III of (3.5) using the observational data JLA + BAO + Planck TT, TE, EE + LowTEB + RSD + WL+ CC + R16.

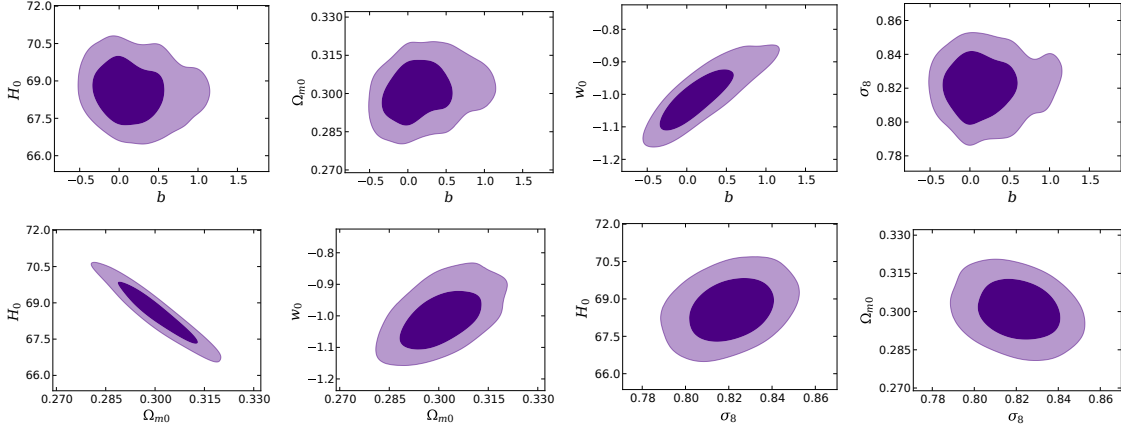


Figure 7. 1σ (68.3%) and 2σ (95.4%) confidence level contour plots for different combinations of the model parameters of Model III of (3.5), for the combined observational data JLA + BAO + Planck TT, TE, EE + LowTEB + RSD + WL+ CC + R16.

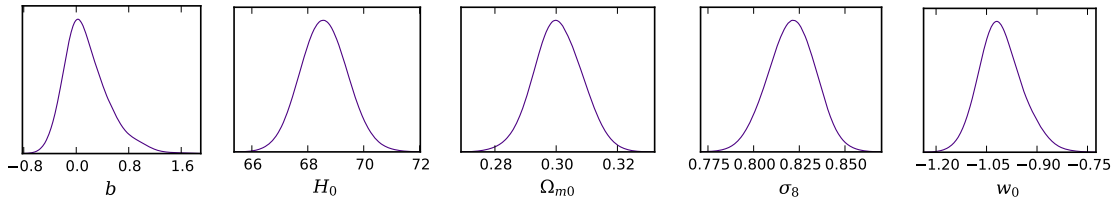


Figure 8. The marginalized 1-dimensional posterior distributions for the model parameters of Model III of (3.5), for the combined observational data JLA + BAO + Planck TT, TE, EE + LowTEB + RSD + WL+ CC + R16.

one can see from Table 4, within 1σ confidence-region the quintessential character of w_0 is not excluded, similarly to Model I. Moreover, from the temperature anisotropy in the

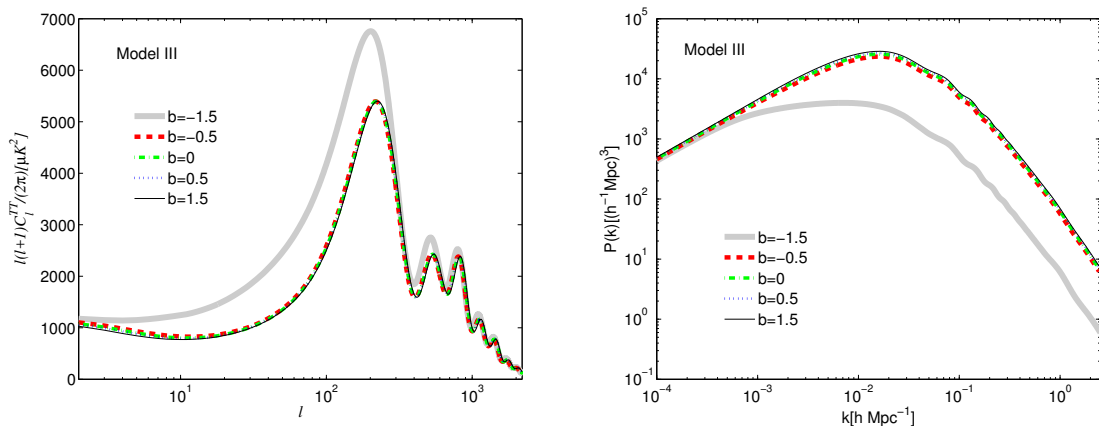


Figure 9. The temperature anisotropy in the CMB spectra (left panel) and the matter power spectra (right panel), for Model III of (3.5), for different values of the parameter b .

CMB spectra and the matter power spectra depicted in Fig. 9, we can see that at large scales, and for large negative values of b (different from Model I and II), the changes in both CMB spectra and matter power spectra, are huge. However, from Table 4 we can see that $-0.0721 < b$ at 3σ confidence level, and thus this exotic behavior is practically not observable. Hence, Model III is close to w CDM cosmology, and thus to Λ CDM cosmology too.

5.4 Model IV

Parameters	Mean $\pm 1\sigma \pm 2\sigma \pm 3\sigma$	Best fit
$\Omega_c h^2$	$0.1182^{+0.0012+0.0023+0.0029}_{-0.0012-0.0023-0.0030}$	0.1182
$\Omega_b h^2$	$0.02231^{+0.00014+0.00028+0.00038}_{-0.00014-0.00028-0.00032}$	0.02233
$100\theta_{MC}$	$1.04063^{+0.00033+0.00061+0.00073}_{-0.00031-0.00062-0.00088}$	1.04024
τ	$0.068^{+0.018+0.032+0.041}_{-0.018-0.035-0.045}$	0.079
n_s	$0.9763^{+0.0040+0.0080+0.0104}_{-0.0039-0.0080-0.0099}$	0.9760
$\ln(10^{10} A_s)$	$3.074^{+0.034+0.063+0.082}_{-0.033-0.067-0.089}$	3.097
w_0	$-1.0270^{+0.0384+0.0641+0.0799}_{-0.0350-0.0651-0.0848}$	-1.0110
b	$0.0641^{+0.1092+0.3054+0.4321}_{-0.1251-0.2469-0.3812}$	0.0428
Ω_{m0}	$0.300^{+0.008+0.016+0.021}_{-0.009-0.015-0.020}$	0.304
σ_8	$0.820^{+0.014+0.029+0.038}_{-0.014-0.027-0.036}$	0.827
H_0	$68.55^{+0.88+1.66+2.22}_{-0.90-1.70-2.06}$	68.20

Table 5. Summary of the observational constraints on Model IV of (3.6) using the observational data JLA + BAO + Planck TT, TE, EE + LowTEB + RSD + WL+ CC + R16.

Finally, for the Model IV of (3.6) we perform the joint analysis and in Table 5 we display the summary of the main observational constraints. Moreover, in Fig. 10 we show the 1σ and 2σ confidence-level contour plots for several combinations of the model parameters and

the derived parameters. Additionally, in Fig. 11 we present the corresponding marginalized one-dimensional posterior distributions for the involved quantities.

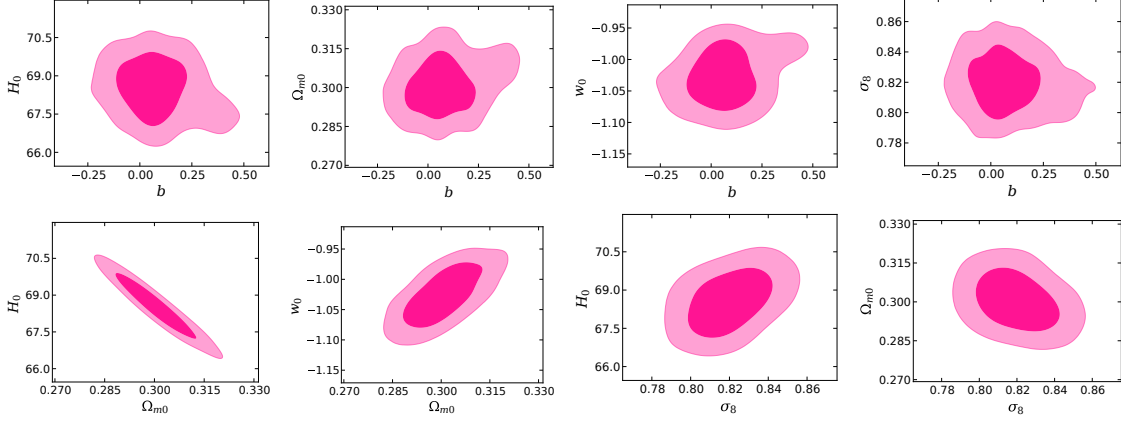


Figure 10. 1σ (68.3%) and 2σ (95.4%) confidence level contour plots for different combinations of the model parameters of Model IV of (3.6), for the combined observational data JLA + BAO + Planck TT, TE, EE + LowTEB + RSD + WL+ CC + R16.

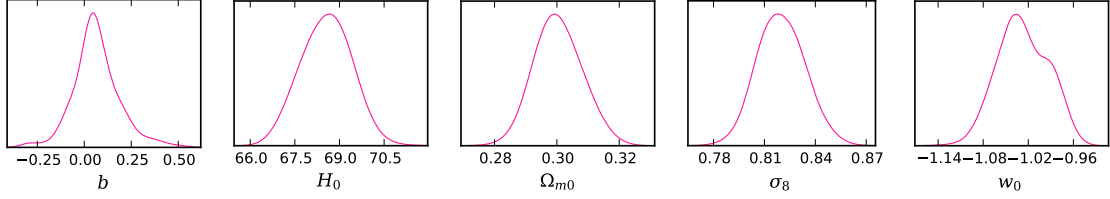


Figure 11. The marginalized 1-dimensional posterior distributions for the model parameters of Model IV of (3.6), for the combined observational data JLA + BAO + Planck TT, TE, EE + LowTEB + RSD + WL+ CC + R16.

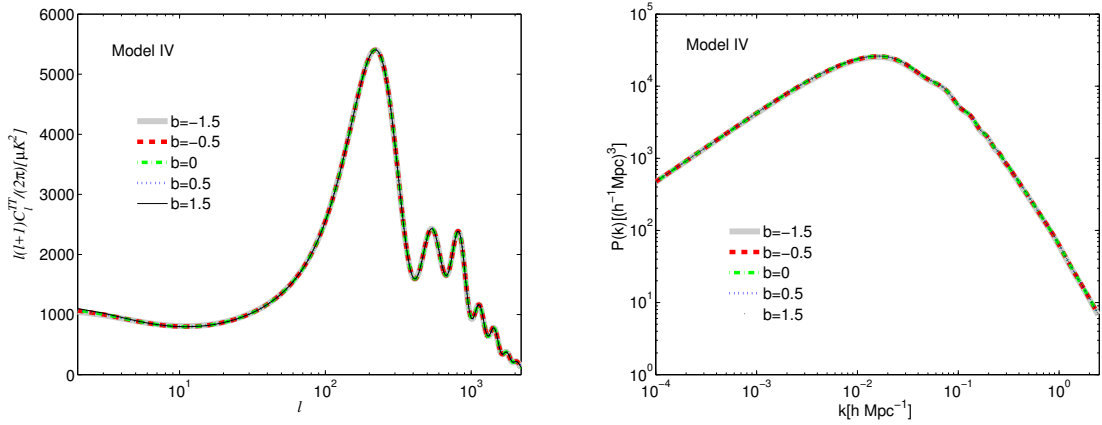


Figure 12. The temperature anisotropy in the CMB spectra (left panel) and the matter power spectra (right panel), for Model IV of (3.6), for different values of the parameter b .

As we can observe, the joint analysis reveals that for the Model IV, both the best-fit and the mean values of the dark-energy equation-of-state parameter at present exhibit phantom behaviour, although very close to -1 , however, as one can see from Table 5, within 1σ confidence-region the quintessential character of w_0 is not excluded, similarly to Model I and Model III. Additionally, from the temperature anisotropy in the CMB spectra and the matter power spectra depicted in Fig. 12, we can see that we do not find any significant variation from w CDM cosmology, and thus from Λ CDM paradigm.

6 Model comparison

In this section we proceed to a comparison of the fittings of the different models, both at background and perturbative levels. In Fig. 13 we present the 1σ and 2σ confidence-level contour plots for several combinations of the free parameters and of the derived parameters, for all Models I-IV simultaneously. As we can observe, Model I is slightly different compared to the other three models, although not significantly. However, focusing on the evolution of the dark-energy equation-of-state parameter presented in Fig. 14, we can see that the difference between the various models becomes very clear. In particular, from the evolution of $w_x(z)$ one can clearly see that Model II and Model III are qualitatively equivalent, while the evolutions of Model I and Model IV are completely different.

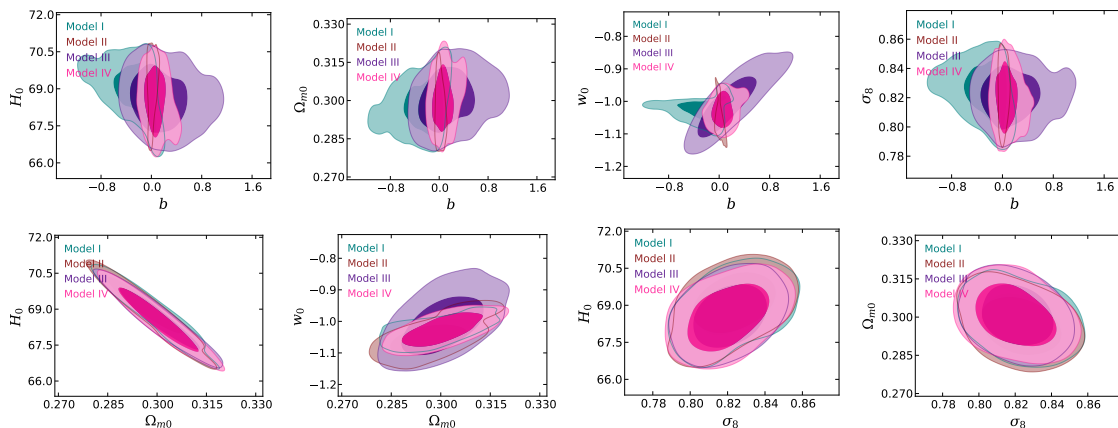


Figure 13. 1σ (68.3%) and 2σ (95.4%) confidence level contour plots for different combinations of the model parameters, for all Models I-IV of (3.3)-(3.6) simultaneously, for the combined observational data JLA + BAO + Planck TT, TE, EE + LowTEB + RSD + WL+ CC + R16.

Moreover, we analyze the trend of the two main parameters of the oscillating models, namely b and w_0 , for different values of H_0 using the MCMC chain of the combined analysis JLA + BAO + Planck TT, TE, EE + LowTEB + RSD + WL+ CC + R16, and in Fig. 15 we present the results for all models. From the analysis of the MCMC chain, one can clearly notice that higher values of H_0 (the red sample points in Fig. 15) favour the phantom behavior of dark energy, while for low values of the Hubble constant H_0 (the blue sample points in Fig. 15) a quintessence-like dark energy is favoured, however within 1σ w_0 is close to -1 . In the latter case, the density of the sample points recommends b to be

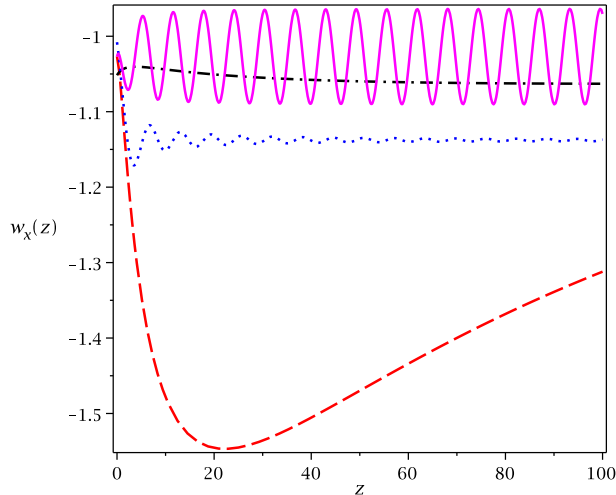


Figure 14. The evolution of the dark-energy equation-of-state parameter $w_x(z)$, for the mean values of (w_0, b) that arise from the combined analysis *JLA + BAO + Planck TT, TE, EE + LowTEB + RSD + WL+ CC + R16*, for Model I of (3.3) (red-dashed), for Model II of (3.4) (black-dash dotted), for Model III of (3.5) (blue-dotted), and for Model IV of (3.6) (magenta-solid).

very close to zero. We mention that the best-fit values of H_0 for all models are attained in between the red and blue regions of the vertical line representing the H_0 values, from which it is again proved that the models are bent towards the phantom region.

In order to examine whether these differences can be observed at large scales, in Fig. 16 we depict the temperature anisotropy in the CMB spectra (left graph) and the matter power spectra (right graph), for all models simultaneously, using for each model the corresponding mean value for the parameter b . From both graphs we deduce that we cannot distinguish the various models, and moreover all models are found to exhibit a behaviour close to that of the flat w CDM scenario. Nevertheless, the model parameter b plays an important role, as can be seen from Fig. 17 where we show the relative deviation of the CMB TT spectrum from the w CDM model (i.e. for $b = 0$) for each model, for different values of b . These graphs show that for large b values the various models deviate from the w CDM model significantly. Similar conclusion can be drawn from Fig. 18, where we present the relative deviation of the matter power spectrum from w CDM cosmology (i.e. for $b = 0$) for each model, for different values of b .

7 Conclusions

Since the nature of the dark energy sector is unknown, one can incorporate its effect in a phenomenological way, i.e. introducing various parametrizations of the dark energy equation-of-state parameter. One interesting parametrization class is the case where $w_x(z)$ exhibits oscillating behaviour [19, 23–28], since it may lead to interesting cosmology.

In order to thoroughly examine whether oscillating dark-energy models are in agreement with the latest observational data, we have performed a complete observational con-

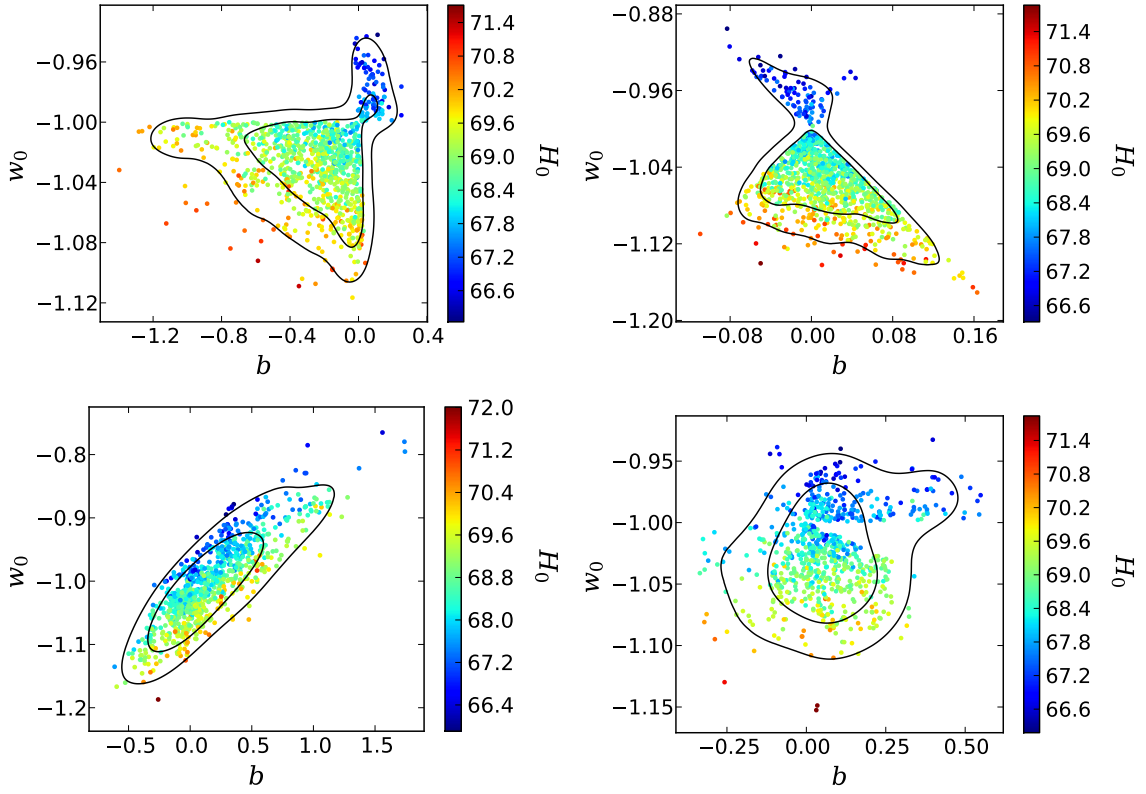


Figure 15. The trend of the key parameters (b, w_0) of the oscillating DE models, namely for Model I of (3.3) (upper left graph), for Model II of (3.4) (upper right graph), for Model III of (3.5) (lower left graph) and for Model IV of (3.6) (lower right graph), for different values of H_0 , from the MCMC chain of the combined analysis JLA + BAO + Planck TT, TE, EE + LowTEB + RSD + WL+ CC + R16.

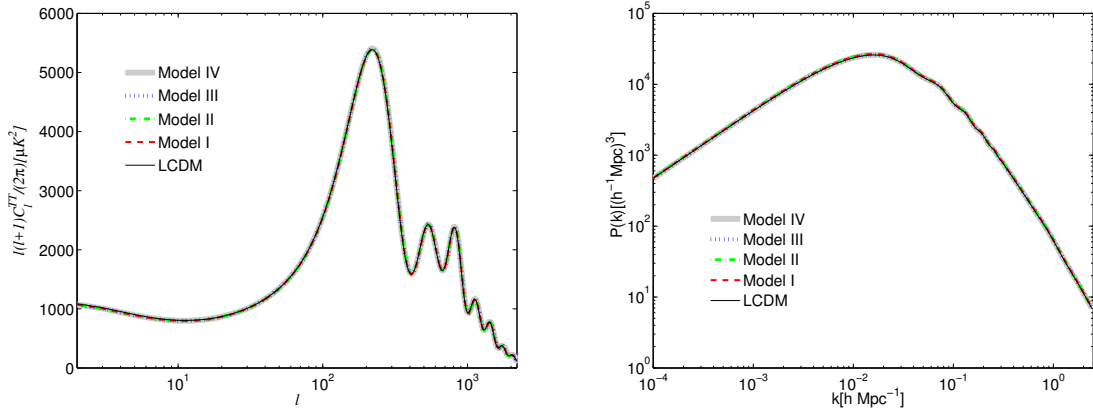


Figure 16. The temperature anisotropy in the CMB spectra (left panel) and the matter power spectra (right panel), for all Models I-IV of (3.3)-(3.6) simultaneously, for the mean values of (w_0, b) that arise from the combined analysis JLA + BAO + Planck TT, TE, EE + LowTEB + RSD + WL+ CC + R16, and the corresponding curves of Λ CDM cosmology.

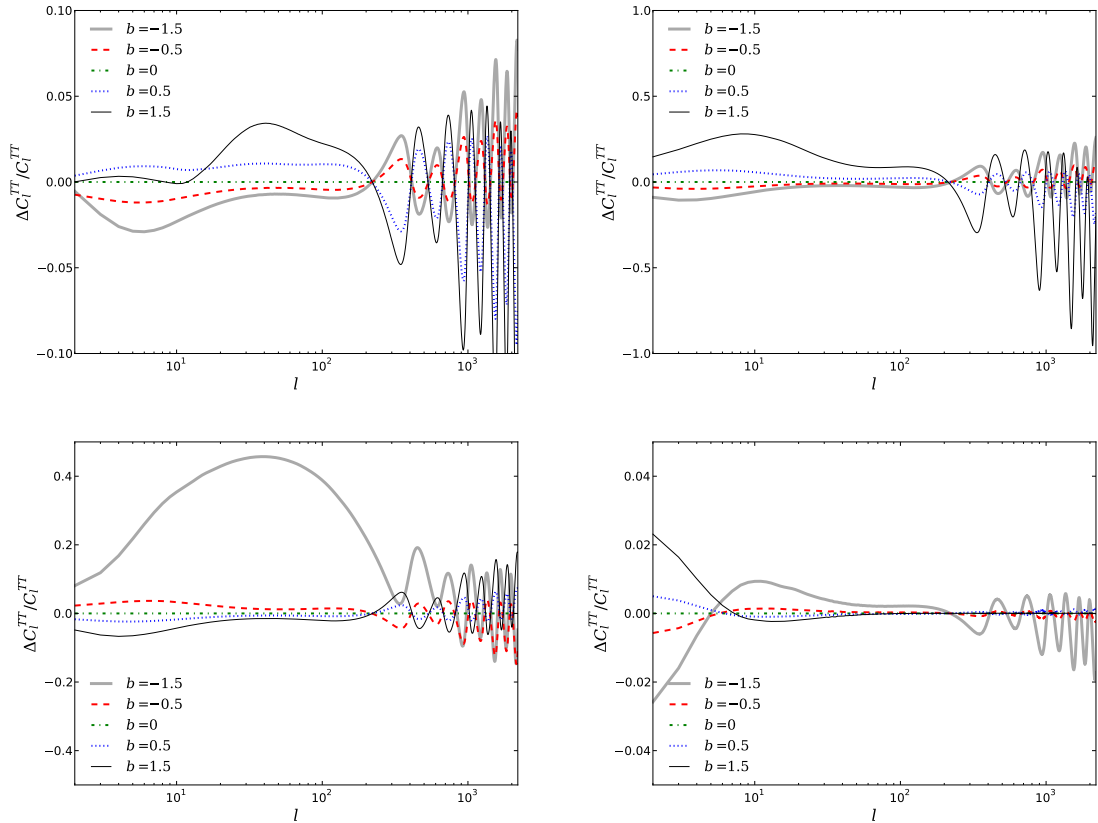


Figure 17. Relative deviation of the CMB TT spectrum from the w CDM model ($b = 0$) for Model I of (3.3) (upper left), for Model II of (3.4) (upper right), for Model III of (3.5) (lower left), and for Model IV of (3.6) (lower right), for different values of b .

frontation using the latest data, namely: Joint Light Curve analysis (JLA) sample from Supernovae Type Ia, Baryon Acoustic Oscillations (BAO) distance measurements, Cosmic Microwave Background (CMB) observations, redshift space distortion, weak gravitational lensing, Hubble parameter measurements from cosmic chronometers, and the local Hubble constant value.

We considered four oscillating dark energy models, namely, Model I of (3.3), Model II of (3.4), Model III of (3.5) and Model IV of (3.6). Our analysis shows that the models are bent towards the phantom region (the best-fit value and the mean value of w_0 for all models are phantom), nevertheless in all models (apart from Model II), the quintessential regime is also allowed within 1σ confidence-level. The models indicate deviations from Λ CDM cosmology, although such deviations are small. The fittings suggest that in all viable oscillating dark-energy models, the parameter b that quantifies the deviation from w CDM and Λ CDM cosmology is relatively small.

As a next step we analyzed the behaviour of the oscillating models at large scales, through the impact on the temperature anisotropy of the CMB spectra and on the matter power spectra. Moreover, we compared the results with the w CDM and Λ CDM scenarios,

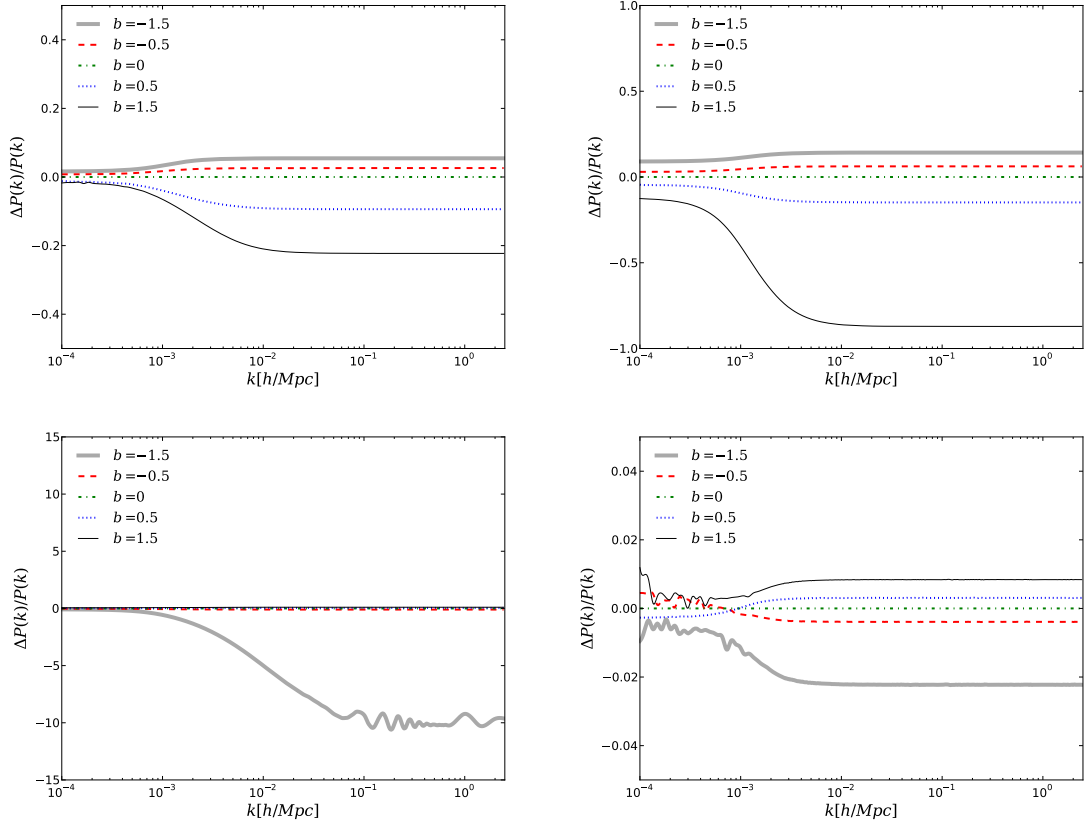


Figure 18. Relative deviation of the matter power spectrum from the w CDM model ($b = 0$) for Model I of (3.3) (upper left), for Model II of (3.4) (upper right), for Model III of (3.5) (lower left), and for Model IV of (3.6) (lower right), for different values of b .

examining the corresponding deviations. As we showed, for Models II and III the deviation from w CDM and Λ CDM models is clear for large negative values of the parameter b . On the other hand, Model I exhibits a slight deviation, while for Model IV the deviation is non-significant.

In summary, the analysis of the present work reveals that oscillating dark energy models can be in agreement with observations. One interesting extension of the above investigation would be to proceed to a more general formalism where the sound speed of the dark energy could be variable, instead of constant. This study could enlighten the intrinsic nature of the oscillating dark energy models, especially in comparison with non-oscillating models. Such an investigation is left for a future project.

Acknowledgments

The research of SP was supported by the SERB-NPDF grant (File No. PDF/2015/000640). SP also thanks the DPS, IISER Kolkata, India, where a part of the work was finished. W. Yang's work is supported by the National Natural Science Foundation of China under Grants No. 11705079 and No. 11647153. This article is based upon work from COST

Action “Cosmology and Astrophysics Network for Theoretical Advances and Training Actions”, supported by COST (European Cooperation in Science and Technology).

References

- [1] E. J. Copeland, M. Sami and S. Tsujikawa, *Dynamics of dark energy*, Int. J. Mod. Phys. D **15**, 1753 (2006), [[arXiv:hep-th/0603057](#)].
- [2] Y. -F. Cai, E. N. Saridakis, M. R. Setare and J. -Q. Xia, *Quintom Cosmology: Theoretical implications and observations*, Phys. Rept. **493**, 1 (2010), [[arXiv:0909.2776](#)].
- [3] S. Nojiri and S. D. Odintsov, *Introduction to modified gravity and gravitational alternative for dark energy*, eConf C **0602061**, 06 (2006) [Int. J. Geom. Meth. Mod. Phys. **4**, 115 (2007)] [[arXiv:hep-th/0601213](#)].
- [4] S. Capozziello and M. De Laurentis, *Extended Theories of Gravity*, Phys. Rept. **509**, 167 (2011), [[arXiv:1108.6266](#)].
- [5] Y. F. Cai, S. Capozziello, M. De Laurentis and E. N. Saridakis, *f(T) Teleparallel Gravity and Cosmology*, Rept. Prog. Phys. **79**, no. 10, 106901 (2016), [[arXiv:1511.07586](#)].
- [6] Y. g. Gong and Y. Z. Zhang, *Probing the curvature and dark energy*, Phys. Rev. D **72**, 043518 (2005), [[arXiv:astro-ph/0502262](#)].
- [7] M. Chevallier and D. Polarski, *Accelerating universes with scaling dark matter*, Int. J. Mod. Phys. D **10**, 213 (2001), [[arXiv:gr-qc/0009008](#)].
- [8] E. V. Linder, *Exploring the expansion history of the universe*, Phys. Rev. Lett. **90**, 091301 (2003), [[arXiv:astro-ph/0208512](#)].
- [9] A. R. Cooray and D. Huterer, *Gravitational lensing as a probe of quintessence*, Astrophys. J. **513**, L95 (1999), [[arXiv:astro-ph/9901097](#)].
- [10] P. Astier, *Can luminosity distance measurements probe the equation of state of dark energy*, Phys. Lett. B **500**, 8 (2001), [[arXiv:astro-ph/0008306](#)].
- [11] J. Weller and A. Albrecht, *Future supernovae observations as a probe of dark energy*, Phys. Rev. D **65**, 103512 (2002), [[arXiv:astro-ph/0106079](#)].
- [12] G. Efstathiou, *Constraining the equation of state of the universe from distant type Ia supernovae and cosmic microwave background anisotropies*, Mon. Not. Roy. Astron. Soc. **310**, 842 (1999), [[arXiv:astro-ph/9904356](#)].
- [13] H. K. Jassal, J. S. Bagla and T. Padmanabhan, *Observational constraints on low redshift evolution of dark energy: How consistent are different observations?*, Phys. Rev. D **72**, 103503 (2005), [[arXiv:astro-ph/0506748](#)].
- [14] E. M. Barboza, Jr. and J. S. Alcaniz, *A parametric model for dark energy*, Phys. Lett. B **666**, 415 (2008), [[arXiv:0805.1713](#)].
- [15] C. J. Feng, X. Y. Shen, P. Li and X. Z. Li, *A New Class of Parametrization for Dark Energy without Divergence*, JCAP **1209**, 023 (2012), [[arXiv:1206.0063](#)].
- [16] L. Feng and T. Lu, *A new equation of state for dark energy model*, JCAP **1111**, 034 (2011), [[arXiv:1203.1784](#)].
- [17] G. Pantazis, S. Nesseris and L. Perivolaropoulos, *Comparison of thawing and freezing dark energy parametrizations*, Phys. Rev. D **93**, no. 10, 103503 (2016), [[arXiv:1603.02164](#)].

- [18] W. Yang, S. Pan and A. Paliathanasis, *Latest astronomical constraints on some nonlinear parametric dark energy models*, [[arXiv:1708.01717](#)].
- [19] J. Z. Ma and X. Zhang, *Probing the dynamics of dark energy with novel parametrizations*, Phys. Lett. B **699**, 233 (2011), [[arXiv:1102.2671](#)].
- [20] E. V. Linder and D. Huterer, *How many dark energy parameters?*, Phys. Rev. D **72**, 043509 (2005), [[arXiv:astro-ph/0505330](#)].
- [21] A. De Felice, S. Nesseris and S. Tsujikawa, *Observational constraints on dark energy with a fast varying equation of state*, JCAP **1205**, 029 (2012), [[arXiv:1203.6760](#)].
- [22] R. J. F. Marcondes and S. Pan, *Cosmic chronometers constraints on some fast-varying dark energy equations of state*, [[arXiv:1711.06157](#)].
- [23] V. Sahni and L. M. Wang, *A New cosmological model of quintessence and dark matter*, Phys. Rev. D **62**, 103517 (2000), [[arXiv:astro-ph/9910097](#)].
- [24] S. Dodelson, M. Kaplinghat and E. Stewart, *Solving the coincidence problem : Tracking oscillating energy*, Phys. Rev. Lett. **85**, 5276 (2000), [[arXiv:astro-ph/0002360](#)].
- [25] B. Feng, M. Li, Y. S. Piao and X. Zhang, *Oscillating quintom and the recurrent universe*, Phys. Lett. B **634**, 101 (2006), [[arXiv:astro-ph/0407432](#)].
- [26] J. Q. Xia, B. Feng and X. M. Zhang, *Constraints on oscillating quintom from supernova, microwave background and galaxy clustering*, Mod. Phys. Lett. A **20**, 2409 (2005), [[arXiv:astro-ph/0411501](#)].
- [27] D. Jain, A. Dev and J. S. Alcaniz, *Cosmological bounds on oscillating dark energy models*, Phys. Lett. B **656**, 15 (2007), [[arXiv:0709.4234](#)].
- [28] R. Lazkoz, V. Salzano and I. Sendra, *Oscillations in the dark energy EoS: new MCMC lessons*, Phys. Lett. B **694**, 198 (2011), [[arXiv:1003.6084](#)].
- [29] S. Nesseris and L. Perivolaropoulos, *A Comparison of cosmological models using recent supernova data*, Phys. Rev. D **70**, 043531 (2004) [[arXiv:astro-ph/0401556](#)].
- [30] V. F. Mukhanov, H. A. Feldman and R. H. Brandenberger, Phys. Rept. **215**, 203 (1992).
- [31] C. P. Ma and E. Bertschinger, *Cosmological perturbation theory in the synchronous and conformal Newtonian gauges*, Astrophys. J. **455**, 7 (1995), [[arXiv:astro-ph/9506072](#)].
- [32] K. A. Malik and D. Wands, *Cosmological perturbations*, Phys. Rept. **475**, 1 (2009), [[arXiv:0809.4944](#)].
- [33] J. K. Erickson, R. R. Caldwell, P. J. Steinhardt, C. Armendariz-Picon and V. F. Mukhanov, *Measuring the speed of sound of quintessence*, Phys. Rev. Lett. **88**, 121301 (2002), [[arXiv:astro-ph/0112438](#)].
- [34] J. Weller and A. M. Lewis, *Large scale cosmic microwave background anisotropies and dark energy*, Mon. Not. Roy. Astron. Soc. **346**, 987 (2003), [[arXiv:astro-ph/0307104](#)].
- [35] S. Hannestad, *Constraints on the sound speed of dark energy*, Phys. Rev. D **71**, 103519 (2005), [[arXiv:astro-ph/0504017](#)].
- [36] M. Betoule *et al.* [SDSS Collaboration], *Improved cosmological constraints from a joint analysis of the SDSS-II and SNLS supernova samples*, Astron. Astrophys. **568**, A22 (2014), [[arXiv:1401.4064](#)].
- [37] F. Beutler *et al.*, *The 6dF Galaxy Survey: Baryon Acoustic Oscillations and the Local Hubble*

- Constant*, Mon. Not. Roy. Astron. Soc. **416**, 3017 (2011), [[arXiv:1106.3366](#)].
- [38] A. J. Ross, L. Samushia, C. Howlett, W. J. Percival, A. Burden and M. Manera, *The clustering of the SDSS DR7 main Galaxy sample I. A 4 per cent distance measure at $z = 0.15$* , Mon. Not. Roy. Astron. Soc. **449**, no. 1, 835 (2015), [[arXiv:1409.3242](#)].
- [39] H. Gil-Marín *et al.*, *The clustering of galaxies in the SDSS-III Baryon Oscillation Spectroscopic Survey: BAO measurement from the LOS-dependent power spectrum of DR12 BOSS galaxies*, Mon. Not. Roy. Astron. Soc. **460**, no. 4, 4210 (2016) [[arXiv:1509.06373](#)].
- [40] R. Adam *et al.* [Planck Collaboration], *Planck 2015 results. I. Overview of products and scientific results*, Astron. Astrophys. **594**, A1 (2016), [[arXiv:1502.01582](#)].
- [41] N. Aghanim *et al.* [Planck Collaboration], *Planck 2015 results. XI. CMB power spectra, likelihoods, and robustness of parameters*, Astron. Astrophys. **594**, A11 (2016), [[arXiv:1507.02704](#)].
- [42] C. Heymans *et al.*, *CFHTLenS tomographic weak lensing cosmological parameter constraints: Mitigating the impact of intrinsic galaxy alignments*, Mon. Not. Roy. Astron. Soc. **432**, 2433 (2013), [[arXiv:1303.1808](#)].
- [43] M. Asgari, C. Heymans, C. Blake, J. Harnois-Deraps, P. Schneider and L. Van Waerbeke, *Revisiting CFHTLenS cosmic shear: Optimal E/B mode decomposition using COSEBIs and compressed COSEBIs*, Mon. Not. Roy. Astron. Soc. **464**, 1676 (2017), [[arXiv:1601.00115](#)].
- [44] R. C. Nunes, S. Pan and E. N. Saridakis, *New constraints on interacting dark energy from cosmic chronometers*, Phys. Rev. D **94**, no. 2, 023508 (2016) [[arXiv:1605.01712](#)].
- [45] F. Anagnostopoulos and S. Basilakos, *Constraining the dark energy models with $H(z)$ data: an approach independent of H_0* , [[arXiv:1709.02356](#)].
- [46] M. Moresco *et al.*, *A 6% measurement of the Hubble parameter at $z \sim 0.45$: direct evidence of the epoch of cosmic re-acceleration*, JCAP **1605**, 014 (2016), [[arXiv:1601.01701](#)].
- [47] A. G. Riess *et al.*, *A 2.4% Determination of the Local Value of the Hubble Constant*, Astrophys. J. **826**, no. 1, 56 (2016), [[arXiv:1604.01424](#)].
- [48] A. Lewis and S. Bridle, *Cosmological parameters from CMB and other data: A Monte Carlo approach*, Phys. Rev. D **66**, 103511 (2002), [[arXiv:astro-ph/0205436](#)].